Near-surface circulation in the Tropical Atlantic Ocean

Rick Lumpkin*, Silvia L. Garzoli

National Oceanographic and Atmospheric Administration, Atlantic Oceanographic and Meteorological Laboratory, Miami, FL 33149, USA

Abstract

A recent data set of surface drifter observations in the tropical Atlantic Ocean is analyzed with a methodology that groups the observations into bins and, within each bin, simultaneously decomposed them into a time-mean, annual and semiannual harmonics, and an eddy residual with non-zero integral time scale. Features of the time-mean circulation and its seasonal variations are resolved at unprecedented scales, for both total and Ekman-removed velocities. The drifter observations reveal the branches of the South Equatorial Current (SEC) which merge with the North Brazil Current (NBC), correlated annual fluctuations in the strengths of the NBC retroflection, western North Equatorial Countercurrent (NECC) and SEC, and flow along the Guyana Coast, and strong semiannual variations in the equatorial band of the central basin. Conduits are traced which link seasonal variations of the equatorial current system's strength with the northern and southern hemisphere subtropical gyres. These findings update key results of the two decade old SEQUAL/FOCAL programs, and allow generation of a new monthly climatology of near-surface currents in the tropical Atlantic Ocean.
Published by Elsevier Ltd.

1. Introduction

The importance of sea surface temperature (SST) variability in the tropical Atlantic as a response to the seasonally varying winds has been the subject of numerous studies. SST in the tropics is largely determined by upper ocean dynamics including advection. Therefore, to understand and model its influence in climate, a clear picture of the surface currents and their variability is necessary. The most comprehensive observational effort to date in the tropical Atlantic was the joint US/French Seasonal Response of the Equatorial Atlantic (SEQUAL) and Programme Francaise Océan-Climat en Atlantique Equatorial (FOCAL) programs of 1983–1985. The follow-up to this effort, Tropical Ocean-Global Atmosphere (TOGA), focused primarily upon the Pacific Ocean. The SEQUAL/FOCAL project incorporated climatological winds and currents, the latter determined from ship drifts. Today's knowledge of the basin wide tropical Atlantic surface circulation is founded upon those early results, supplemented by more recent observations and analyses.

*Corresponding author.

The tropical Atlantic surface circulation (Fig. 1; for a recent review, see Stramma et al., 2003) is bounded by the equatorial edges of the northern and southern hemispheres' subtropical gyres, including the westward North and South Equatorial Currents (SECs) which feed poleward western boundary currents (the Gulf Stream and the Brazil Current). Breaking this symmetry, the SEC flows westward towards the Brazilian Coast where it bifurcates into the cross-equatorial North Brazil Current (NBC) to the north and the Brazil Current to the south.

The NBC is the western boundary of the wind-driven gyre in the tropical Atlantic. From its origin at the bifurcation of the SEC, the NBC flows northward along the Brazilian coast, continuously increasing its transport via input from the SEC. After crossing the equator, a component of the NBC retroflects eastward into the Equatorial Undercurrent, and the remainder of the NBC continues northwestward until it retroflects at approximately $7°N$, $48°W$. At its retroflection, rings are shed which propagate northwestward along the Guyana coast (Didden and Schott, 1993; Wilson et al., 2002); these rings may be responsible for more than half of the interhemispheric exchange of mass and heat associated with the meridional overturning circulation's upper limb (Garzoli et al., 2003).

These net interhemispheric exchanges are masked by shallower overturning cells (cf. Zhang

et al., 2003) superimposed upon a predominantly isopycnal clockwise gyre which dominates the equatorial surface circulation. This equatorial gyre consists of the NBC and its retroflection, the eastward North Equatorial Countercurrent (NECC), the eastern extension of the NECC south of the Guinea Coast of Africa (the Guinea Current, Arnault, 1987) and branches of the SEC which form or join with the NBC.

Early studies (Molinari, 1983; Richardson and McKee, 1984) suggested that tropical Atlantic currents display strong seasonal variability. This variability was studied extensively during the SEQUAL/FOCAL field (cf. Reverdin and McPhaden, 1986) and modeling (Philander and Pacanowski, 1986) programs. Twenty-three near-surface drifting buoys were deployed in the eastern tropical Atlantic as part of SEQUAL/FOCAL with observations spanning the period June 1983–February 1985. Analysis of the seasonal variability revealed by these observations was complemented by historical ship drift observations (Richardson and Walsh, 1986; Richardson and Reverdin, 1987). Subsequent studies using Geosat and TOPEX/Poseidon altimetry (Carton and Katz, 1990; Katz et al., 1995; Arnault et al., 1999) have refined these results by examining the variability of surface geostrophic currents away from the continental shelves (where tidal errors contaminate the altimetric signal).

The most prominent seasonal variations are found in the western NECC (Garzoli and Katz, 1983; Richardson and Walsh, 1986; Richardson and Reverdin, 1987; Arnault, 1987; Garzoli, 1992; Katz et al., 1995) and the equatorial branch of the SEC (Katz et al., 1981; Richardson and Reverdin, 1987; Arnault et al., 1999), which are strongest during boreal fall and weaken or even reverse in spring. Strong seasonality is also displayed by the North Brazil and Guyana Currents (Arnault, 1987; Johns et al., 1998), and in the strength of the NBC retroflection which peaks in boreal summer and fall (Richardson and Walsh, 1986; Richardson and Reverdin, 1987). In the center of the basin, the NECC and equatorial branch of the SEC are strongest during boreal summer (Peterson and Stramma, 1991; Richardson et al., 1992). All these variations are driven by large-scale
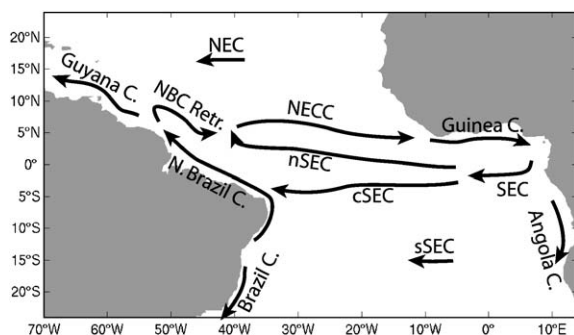

Fig. 1. Schematic of time-mean near-surface currents (arrows) calculated from drifter observations, including, the North Equatorial Current NEC, NECC, northern, central and southern branches of the SEC, and the North Brazil Current and its retroflection (NBC Retr.).

seasonality in the trade winds and the latitude of the intertropical convergence zone (ITCZ) (Philander and Pacanowski, 1986; Stramma and Schott, 1999).

In this paper, the surface circulation of the tropical Atlantic Ocean is analyzed using a recent set of drifting buoy observations. These data are reviewed in Section 2, the methodology used for the analysis is described in Section 3, time-mean currents are presented in Section 4, their seasonal variations in Section 5, results are summarized in Section 6, and conclusions are presented in Section 7.

2. Drifters in the tropical Atlantic Ocean

The increasing database of Surface Velocity Program (SVP) drifting buoy (hereafter "drifter") observations offers an invaluable tool for examining near-surface circulation (World Climate Research Program, 1988; Sybrandy and Niiler, 1992; Niiler, 2001). These drifters have a holey-sock drogue of length 6.4 m and diameter 0.9 m, centered at a depth of 15 m, designed to minimize slip with respect to flow integrated over drogue depths. The drogue's evenly-spaced holes reduce vortex shedding, so that its drag coefficient does not abruptly change across a critical Reynolds number (Nath, 1977). The drogue is tethered to a spherical surface float, which includes a transmitter for location, a thermistor for sea surface temperature, and a submergence sensor used to detect if/when the drogue is lost.

This study analyzes observations from these drifters in the tropical Atlantic domain 24°S–24°N, 70°W–14°E (Fig. 2). The database of quality-controlled, kriged (see Section 3) drifter observations spans the period 28 October 1990–28 February 2004, and consists of 728 drifters which provided 404 drifter-years of observations, 86% of which was collected by the 583 drifters deployed within the tropical Atlantic domain. An additional 84 drifters deployed north of 24°N also entered the domain and passed westward in the North Equatorial Current, re-exiting the domain across 24°N or across 70°W, north of Hispañola. From the south, 61 drifters entered the domain across 24°S and traveled westward in the SEC.

2.1. Evolution of the drifter observing network

For many years, efforts to seed the world's oceans with SVP drifters focused on the Pacific and subtropical/subpolar North Atlantic, while the tropical Atlantic remained nearly bereft of observations (e.g. Fig. 4.1.4 of Niiler, 2001). Prior to late 1997, observations in the tropical Atlantic came from intermittent deployments of drifters in regional clusters, resulting in highly inhomogeneous sampling on the basin-scale. The subsequent evolution of an observing network of drifters has extended the database both spatially and temporally, and allowed studies of these observations to extend from synoptic snapshots of particular currents to the estimates of gyre-scale circulation and its seasonal variability presented here. As the network continues to be maintained, resolution of interannual variability and low-frequency climate fluctuations will become possible from these in situ measurements.

The first deployments of SVD drifters in the tropical Atlantic domain were conducted in late October 1990, when two were placed in the NBC (Richardson et al., 1994). Subsequent deployments through 1995 were limited to the subtropical boundaries of the domain (±18–25°). The situation improved considerably in 1996; in Spring, two drifters were placed in the NBC and two off the Angola coast of Africa. In mid-July 1996, a cluster of 7 drifters was deployed by AOML on a 5° grid at 10–15°N, 30–45°W. At the end of June 1997, a dense array of 10 drifters was placed in and around a tropical instability wave at 1–5°N, 20–23°W (Menkes et al., 2001).

Since August 1997, approximately 80 tropical Atlantic deployments per year have been coordinated by AOML's Global Drifter Center, which uses ships of opportunity and research vessels to maintain a worldwide observing system of these drifters. This program is currently funded as part of the sustained NOAA Global Ocean Observing System for climate. Future deployments will improve coverage in sparsely sampled regions such as the eastern tropical Atlantic, and will resolve interannual variability on a nominal 5° grid. This program has succeeded in creating a true array of drifters in recent years, as opposed to
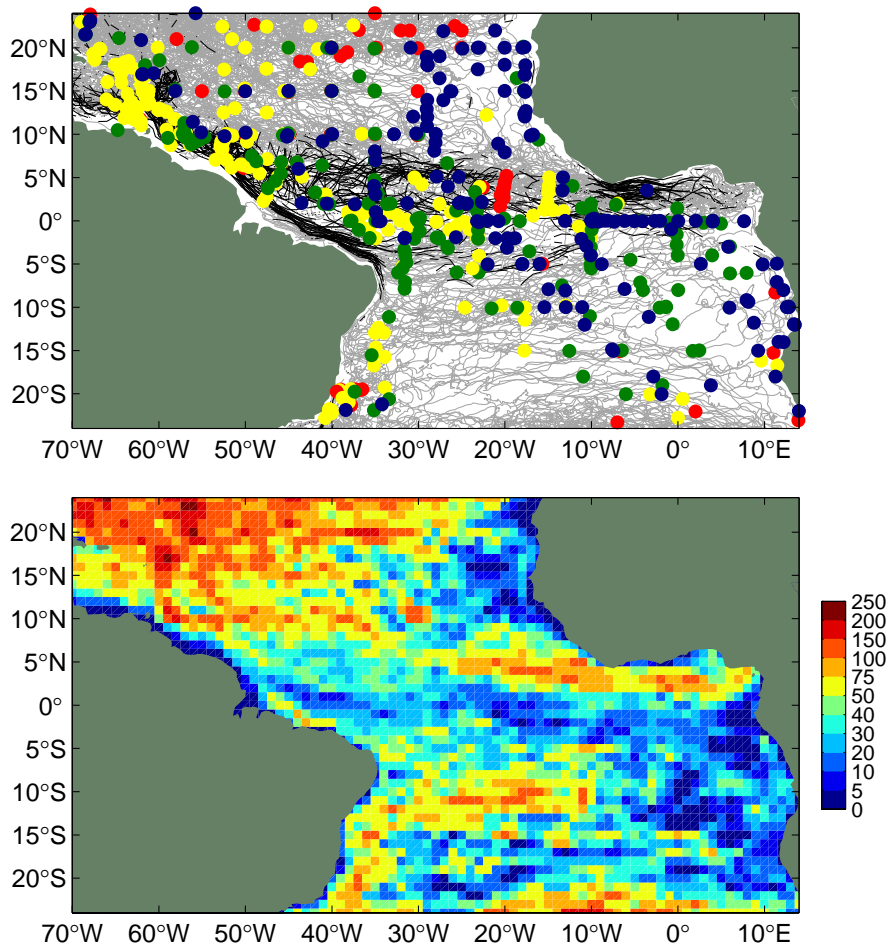
Fig. 2. *Top*: Trajectories of drifters moving at speeds <50 cm/s (light gray) and faster (black). Deployment locations are indicated by colored bullets: 1990–1997 (red), 1998–1999 (yellow), 2000–2001 (green) and 2002–February 2004 (blue). Some recent deployments overlay older ones. *Bottom*: Density of observations (drifter days per square degree).

the patchy coverage offered by regional clusters. More recently, this effort was supplemented by deployment of a ''Hurricane Array'', initiated in 2001 and continued during subsequent hurricane seasons. This array is composed of 10–12 drifters, deployed in the tropical Atlantic and in the hurricane alley regions to the west (outside the domain of this study, but incorporated if they entered the domain). Regional clusters have continued to be deployed, greatly magnifying observation density in some areas. An example of this is the NBC Rings Experiment of November 1998–June 2000, which included dense drifter deployment in the region of the

NBC retroflection and Guyana Current (Glickson et al., 2000).

2.2. Spatial and temporal density of drifter observations

The spatial density of all drifter observations in the domain (Fig. 2, bottom) is highly inhomogeneous, due to the inhomogeneous distribution of deployments and the subsequent pathways of surface advection, i.e. little time spent in regions of surface divergence. The temporal distribution of the observations (Fig. 3) emphasizes the recent increase in observations. Over 88% of the
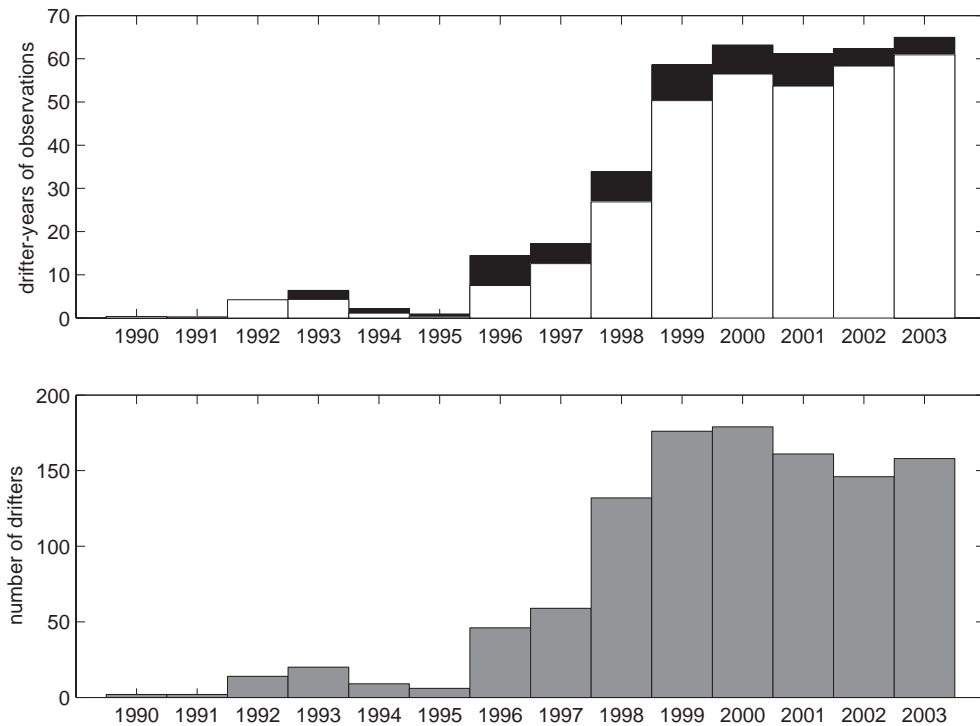
Fig. 3. Temporal distribution of drifter observations in the study domain, 1990–2003. *Top*: number of drifter years, for all drifters (black) and those with drogues attached (white). *Bottom*: number of unique drifters.

observations in the domain were made after 31 December 1997, 66% after 1999, and 50% after 2000. As a consequence, "time-mean" fields derived in this study represent an annual average for the most recent 6 years. Little can yet be said about interannual variability from these data alone, and only now does the spatio-temporal coverage allow estimates of robust means with respect to their seasonal variability.

3. Methodology

3.1. Quality control and interpolation

A drifter's position is estimated from the Doppler shift of its transmission by algorithms which occasionally locate the instrument on the wrong side of a close satellite pass (Poulain and Niiler, 1989; Lumpkin, 1998). To eliminate these more egregious errors in the raw satellite fixes, the Drifting Buoy Data Assembly Center (DAC) of AOML applies a quality evaluation scheme (Hansen and Poulain, 1996) based on the drifter's velocity history. The DAC identifies the dates of each drifter's deployment, drogue loss, and termination of reliable/useful transmissions. These observations are then interpolated to quarter-day intervals via kriging (Hansen and Herman, 1989), using fractional Brownian autocorrelation structure functions for position (Hansen and Poulain, 1996). This technique provides formal error bars for position. The DAC also calculates zonal and meridional speeds via a half-day, centered finite difference of the quarter-day interpolated positions.

3.2. Wind slip and Ekman drift

Slightly over 10% of observations were collected by drifters which had lost their drogues. Due to the relatively sparse coverage in parts of the domain, recovery of this data was considered desirable.

Wind slip was removed from the drogued and undrogued drifter velocities by interpolating daily National Centers for Environmental Prediction (NCEP)/National Center for Atmospheric Research (NCAR) reanalysis winds onto the drifter positions and using the coefficients of Niiler and Paduan (1995) (drogued) and Pazan and Niiler (2000) (undrogued, relative to drogued). Mean currents calculated independently from the slip-removed drogued and undrogued velocities (not shown) displayed no systematic differences in magnitude or direction, with respect to mean wind speed and direction. After removing the slip, the velocities and corresponding wind stresses (also from daily NCEP) were lowpassed at 5 days to remove inertial and tidal components. Kriged locations (and concurrent velocity) with errors greater than $0.03°$ (~ 3.3 km) were typically associated with interpolation across large transmission gaps; these data were discarded. The remaining set of slip-removed, lowpassed velocities will be referred to as the "total" velocities, to distinguish them from the Ekman-removed velocities (see below).

The Ekman component of velocity for each drifter was calculated from the interpolated, lowpassed NCEP wind stresses, using the empirical model of Ralph and Niiler (1999) with updated coefficients (Niiler, 2001). In the study domain, the time-mean Ekman depth scale H_* ranges from <10 m off the Senegal Coast of Africa (where wind stress along the time-mean ITCZ is <0.01 N/m^2) to a maximum of 40 m in the NBC. Currents at upper-thermocline depths beneath this Ekman layer can be estimated by subtracting the Ekman component of the velocity from the total velocity. More precisely, this residual, which we shall call the "Ekman-removed velocity," is due to geostrophic motion at 15 m, non-Ekman ageostrophic motion remaining after lowpassing, and errors in the Ekman model which include biases in the NCEP wind fields.

To test the sensitivity of the Ekman model to variations between different wind products, time-mean Ekman currents were calculated using the fixed coefficients and winds from three products: the time-mean NCEP/NCAR fields, a reanalysis of the Comprehensive Ocean-Atmosphere Data Set

(COADS; Josey et al., 2002) and the 15-year reanalysis of the European Centre for Medium-Range Weather Forecasts (ECMWF). Niiler (2001) calculated these coefficients from drifter/NCEP correlations; it is possible that coefficients calculated from drifter/COADS or drifter/ECMWF correlations might adjust to match systematic wind field differences. Thus, as an error bar the differences between the three sets of Ekman velocities (Fig. 4) will be an upper bound. The differences in magnitude are small compared to errors in time-mean currents from other sources (e.g., sampling), although systematically weaker tropical winds in the NCEP product yield weaker Ekman currents (averaging 0.8 cm/s weaker than COADS, and 1.0 cm/s weaker than ECMWF). There is a significant directional difference between NCEP-derived Ekman currents and currents derived from the other two products in the latitude band 2–8°N, where NCEP currents are $7°$ to the left of the COADS or ECMWF currents. In non-zonally averaged fields, this difference exceeds $10°$ in several bins near the African coast. These differences are used here as a proxy for the error bar on the Ekman component, with the caveat that systematic, consistent biases in all three wind products may introduce additional but unquantified contamination.

3.3. Decomposition of the observations

To derive pseudo-Eulerian estimates from the Lagrangian observations, the observations are grouped in spatial bins and, within each bin, treated as a time series composed of a time-mean value, annual and semiannual harmonics, and residual $n(t)$, using inverse techniques (Lumpkin, 2003). In this approach, the covariance structure of the residual is specified, which can include a non-zero integral time scale. For this study, a time scale of 5 days was used; within a bin, the quarter-day interpolated current measurements are not treated as independent if separated by less than this time scale. Because the methodology explicitly includes seasonal harmonics when decomposing the observations, it avoids biasing the means where the seasonal cycle is strong and the observations are inhomogeneously distributed
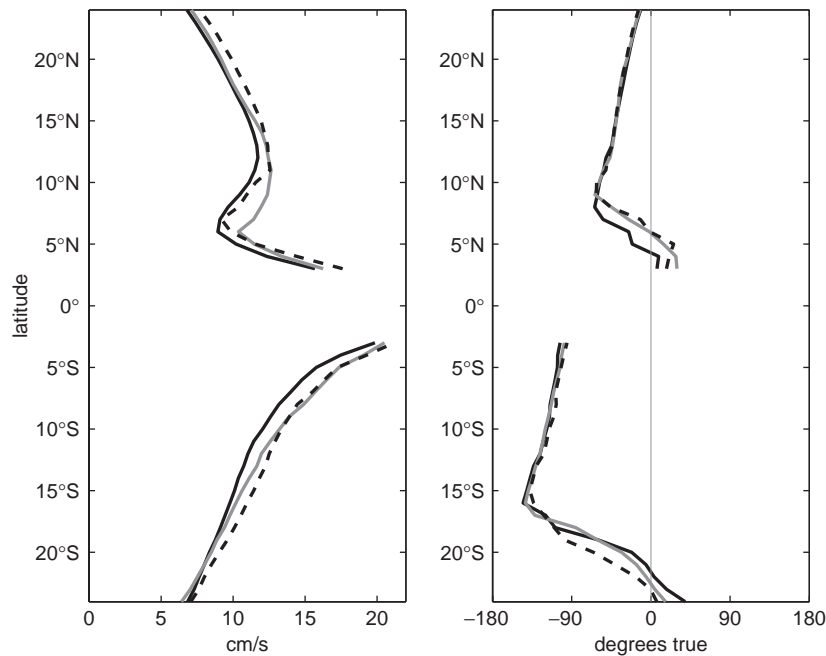
Fig. 4. Zonally averaged magnitude (left) and direction (right; 0° = north) of Ekman velocity from the Ralph and Niiler (1999) parameterization applied to time-mean winds from NCEP/NCAR Reanalysis 2 (solid black), Southampton reanalysis of the Comprehensive Ocean-Atmosphere Data Set (gray) and the 15-year reanalysis of ECMWF (dashed black).

through the seasons. It also produces large error bars on the mean and seasonal amplitudes if a bin contains many observations, but all within a particular season, as can happen with "batch" deployments from one or two seasonally coincident cruises.

The methodology was tested using simulated drifters in a $1/12°$ simulation of the tropical Atlantic Ocean. Results (Lumpkin and Garraffo, 2005) demonstrate that the methodology can successfully resolve the mean currents and its seasonal variations throughout most of the tropical Atlantic with the present density of observations, that the mean values are less biased than those obtained by simple binned averaging, and that the error bars are appropriately sensitive to both the overall density and the seasonal homogeneity of observations within a bin.

3.4. Spatial resolution of the pseudo-Eulerian maps

Our goal is to map the spatial distribution of currents at a nominal resolution of $1° \times 1°$.

Various choices of bin size were evaluated using numerical model output with realistic tropical Atlantic drifter observation density (Lumpkin and Garraffo, 2005); the two-iteration scheme described below yielded smaller RMS errors than simply applying the methodology to data grouped in $1° \times 1°$ bins (as in Lumpkin, 2003) or $2° \times 2°$ bins.

The data were initially grouped in $2° \times 2°$ bins, overlapping by $1°$ such that the bin centers lay on a $1° \times 1°$ grid. Within each $2° \times 2°$ bin, the decomposition was performed as described in Lumpkin (2003). The decomposition yielded "prior" estimates of the unknowns (time-mean value plus amplitudes and phases of the seasonal harmonics).

The observations were then grouped in $2° \times 1°$ bins, centered on the same $1° \times 1°$ grid and rotated so that the bins were aligned with the major axis of total velocity variance (Fig. 5). This bin choice tended to spatially average the observations along the path of mean trajectories (and thus along, rather than across, major currents) while including
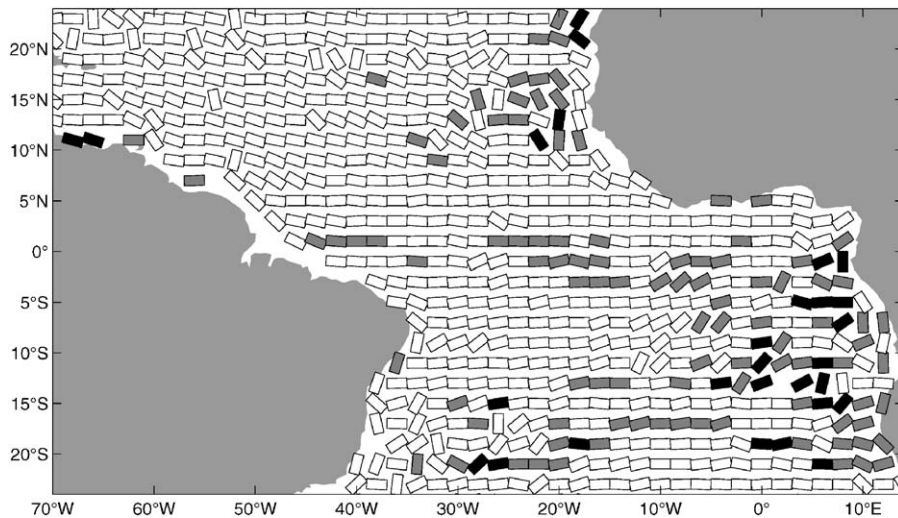
Fig. 5. $2° \times 1°$ bins used to average drifter observations. Bin orientation is set by a principle component analysis of the velocity variance. Every other bin on the $1° \times 1°$ grid is shown. Unshaded bins contain >20 observations per square degree; gray bins contain 5–20 observations; black bins contain <5 observations.

more observations than in $1° \times 1°$ bins. The rotated bins were generally oriented zonally in the interior, particularly in the band $7°S–7°N$, and along the coastlines near South America and Africa. To estimate the error in this orientation angle, the velocities were bootstrap resampled 100 times within each bin. The standard deviation of the angle varied by $15°$ for bins with 5–10 drifter days per square degree of observations, by $8°$ for 10–20 observations, and by $6°$ for >20 observations. Within the rotated $2° \times 1°$ bins, a second iteration of the decomposition was performed for the residual of the total time series and the prior fit from the $2° \times 2°$ bins. Elements of the noise covariance matrix were calculated from the total variance of the time series in the bin, rather than the variance about the prior fit (which would yield spuriously small error estimates).

Two caveats of this least squares approach must be stated explicitly. The seasonal signal is assumed to be captured to lowest order by an annual and semiannual harmonic. At basin scales, these two harmonics account for $\sim 70\%$ of the seasonal variance (Richardson and Walsh, 1986). However, if there are regions with energetic seasonal variations at other frequencies, errors may result in the decomposition. The method also does not expli-

citly treat variability at frequencies lower than annual. Thus, in addition to mesoscale fluctuations, the residual will include interannual variations where the observations can resolve them. Where they cannot, interannual variability may alias the decomposition. For example, the equatorial Pacific is most heavily sampled by surface drifters during El Niño-related warming events, requiring regression onto an ENSO index to yield unbiased mean current estimates (Johnson, 2001).

4. Time-mean currents

The time-mean (annual averaged) currents derived by decomposition of the drifter observations are shown in Fig. 6. The tremendous recent increase in drifter observations permits resolution of mean circulation over much of the tropical Atlantic, in contrast to earlier studies of these data—even quite recently (e.g., Plate 6 of Fratantoni, 2001) the observational density was insufficient to resolve the different branches of the SEC and its bifurcation against the Brazilian coast, features now present in Fig. 6. Even with the recent increase in observations, these data remain too sparse to estimate reliable means in the far
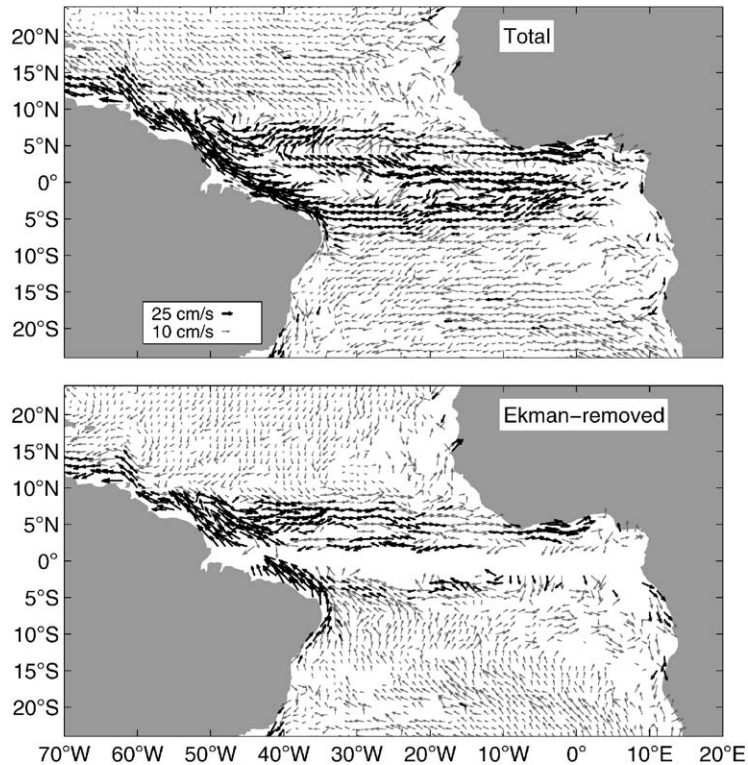
Fig. 6. Time-mean near-surface currents derived from satellite-tracked drifter trajectories. *Top*: total currents. *Bottom*: Ekman-removed currents.

eastern tropical/subtropical boundaries, such as in the Angola Dome where the southward Benguela Coastal Current cannot be observed.

Quiver plots of near-surface currents (Fig. 6) emphasize the strong zonal and western boundary currents. To visualize gyre-scale advective pathways, the trajectories of simulated particles were calculated by integrating along the time-mean current fields (Fig. 7). In the band 2°S–2°N, where the Ralph and Niiler (1999) Ekman model does not apply, the parameterization of Lagerloef et al. (1999) (their Eq. (5), with $h = 32.5\,\text{m}$ and $r = 2.15 \times 10^{-4}\,\text{m s}^{-1}$) was used to derive time-mean Ekman currents. The particles were "released" on a regular 4° grid. Although many of the streamlines in the total (Ekman-included) field resemble trajectories of actual drifters, we stress that this figure should be viewed as a schematic of the mean flow (e.g., to be compared with Fig. 2 of Arnault, 1987), as it does not include the effect of

variability upon the trajectories of actual oceanic parcels. For example, parcels advected in the time-varying Ekman-removed NBC could penetrate the retroflection "barrier" (Fig. 7, bottom) via ring separation and propagation. Similarly, closed (infinitely long) trajectories are found between the Guinea Current and the northern SEC, where eddy-driven dispersion may set a relatively short residence time.

NBC: In the total velocity field, the southern branch of the South Equatorial Current (sSEC) flows southwestward to the Brazilian Coast, where it bifurcates at 12–14°S. North of this, a weak but significant northeastward coastal current gains strength as it is fed by SEC inflow, rounds the easternmost tip of Brazil, and is joined by the central SEC (cSEC) at ∼ 4°S. The confluence of these currents (not present in Fratantoni, 2001 or Zhang et al., 2003) marks a strong acceleration in the NBC, from 55–60 cm/s at 4°S, 36°W to
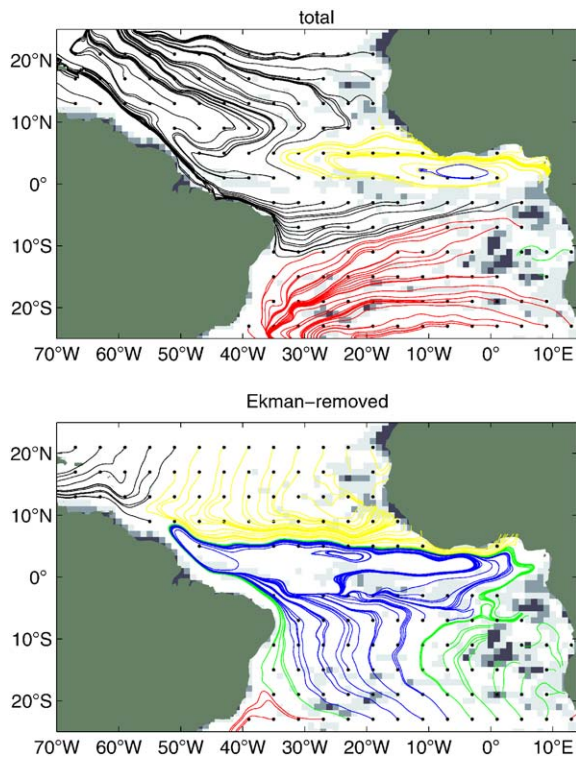
Fig. 7. Trajectories of simulated particles released in the time-mean currents. *Top*: total currents. *Bottom*: Ekman-removed currents. Colors indicate whether the particles exited the integration domain to the northwest (black), to the south (red), if they recirculated indefinitely (blue), or if they entered regions of low observation density in the northern (yellow) or southern (green) hemisphere. Background shading indicates regions of sparse data coverage in the bins: no observations (dark gray), 1–5 drifter days/degree^2 (medium gray), 6–20 drifter days/degree^2 (light gray).

78–88 cm/s at 3°S, 39°W. An extension of the nSEC joins the NBC at 2–3°N, 45–46°W. The fastest (>90 cm/s) time-mean drifter speeds in the domain are found in the NBC, at 46–54°W, consistent with SEQUAL/FOCAL drifter observations (Richardson and Reverdin, 1987). The maximum mean speed, 96.7 ± 7.8 cm/s, is found at 4°N, 49°W. These very large speeds are presumably associated with the confluence of the NBC and the nSEC, and possibly recirculation from the NBC retroflection back into the NBC (seen in the Ekman-removed currents at 2–4°N, 41–43°W; Fig. 6, bottom). Further northwest (50–54°W), the

mean NBC retroflects eastward with speeds of 45–60 cm/s along 44–50°W. At the bin size chosen for this study (and in Fratantoni, 2001), the separation of the retroflection from the coast is clearly resolved in the time-mean field, in contrast to more heavily smoothed fields (Richardson and Walsh, 1986; Zhang et al., 2003).

Guyana Current: The 40–50 cm/s Guyana Current extends from the western edge of the NBC to immediately west of the Windward Islands, where a branch separates from the South American coast to follow the Lesser Antilles arc northward. This branch can be primarily attributed to the time-averaged pathway of NBC retroflection rings, as discussed later. In the total current field, this branch continues to the southern Sargasso Sea. In Ekman-removed currents, it wraps around the northern Leeward Islands and enters the Caribbean Sea southeast of Puerto Rico.

NECC: Time-mean velocities have an eastward component across the entire basin, from the mean NBC retroflection at 5–8°N, 45–50°W to the eastern Guinea Current at 2–4°N, 9°E.

In the total (Ekman included) velocity field the NECC is not a continuous advective pathway (Fig. 7, top). Instead, persistent northward drift along 35–40°W carries parcels out of the western NECC and into the southern edge of the northwestward NEC. The lack of a continuous advective pathway here is not nearly as dramatic as in the mean current fields presented by Fratantoni (2001) or Zhang et al. (2003), due to differences in analysis techniques. The region was heavily sampled during boreal spring and summer months (not shown), when the meridional component is smallest. Results closer to Fratantoni's Fig. 3 can be replicated by bin averaging, rather than performing the least-squares decomposition which includes the seasonal harmonics. Mean ship drifts more closely resemble the results derived in this study (Richardson and Walsh, 1986), perhaps due to more seasonally homogeneous sampling by the ships. This advective path discontinuity is consistent with the large number of SEQUAL/FOCAL drifters which left the NECC and entered the NEC (Richardson and Reverdin, 1987); many comparable recent examples can be found in the SVP drifter database. The western NECC discontinuity

is only a feature of the uppermost water column, as it is not present in the Ekman-removed current field (Figs. 6 and 7, bottom). In this field, the NECC is a continuous advective pathway spanning the tropical Atlantic.

East of 35°W, the uppermost NECC is fed by recirculation from the northern SEC, forming an elongated recirculating NECC/nSEC gyre (Fig. 6, top) consistent with several SEQUAL/FOCAL drifter trajectories (Richardson and Reverdin, 1987). In numerical models, this northward motion is also balanced by subsurface, thermocline-depth flow from 3°N to the equator, forming a shallow overturning cell (Philander and Pacanowski, 1986).

In the central Atlantic (20°W), the NECC has a mean zonal speed which peaks at 22 ± 5 cm/s at 4°N (Fig. 8; 19 cm/s Ekman-removed). Upon encountering and passing south of the African coast at 10–15°W, the eastern NECC accelerates and forms the coastal Guinea Current, with a mean speed of 65 ± 8 cm/s (57 cm/s Ekman-removed) at 3–6°W. East of 5°W, southward currents along 1–3°N indicate recirculation from the Guinea Current to the westward jets of the SEC (Fig. 6).

SEC system: Within the equatorial gyre system, the mean SEC is clearly divided into two westward jets, the nSEC and the cSEC, separated at 0–2°S by a band of weak, southward mean velocities. This two-core structure is not well-resolved in smoothed fields (Richardson and Walsh, 1986; Zhang et al., 2003), but it is a robust feature of the equatorial SEC seem in hydrography (Molinari, 1982) and in SEQUAL/FOCAL drifter trajectories (Richardson and Reverdin, 1987).
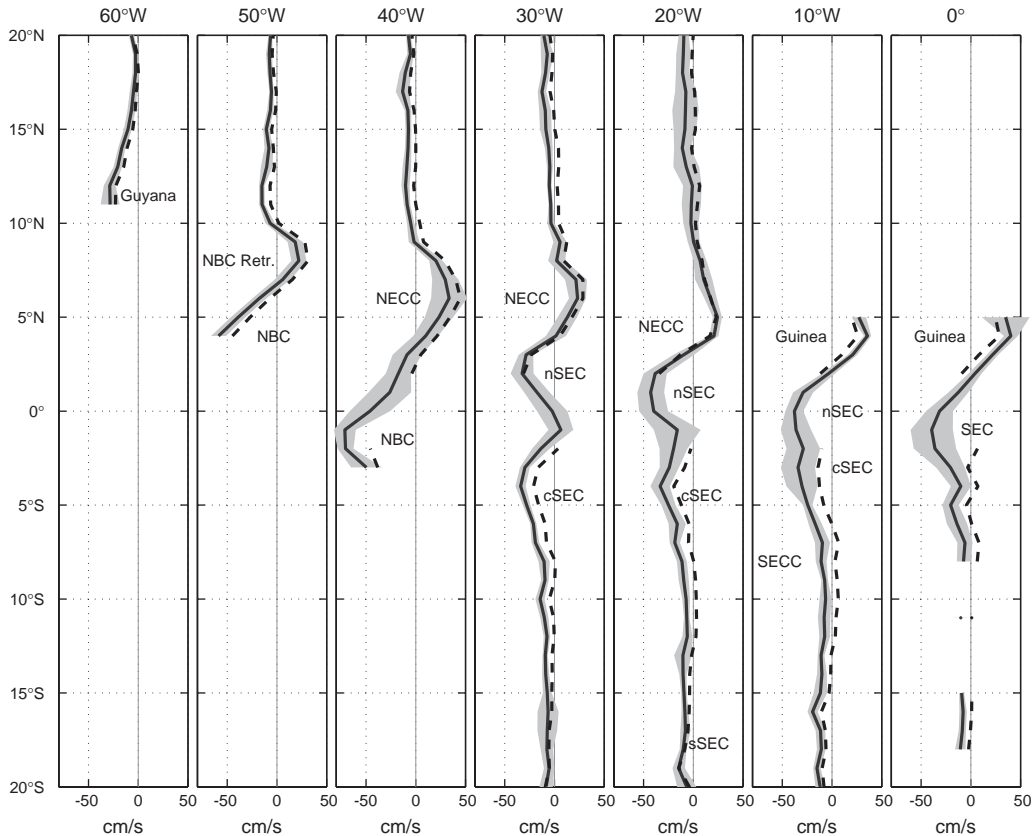

Fig. 8. Solid curves: time-mean zonal speed of drifters, zonally averaged in 5° bands (center longitude given in title of each panel). Shading: standard error. Dashed curves: Ekman-removed mean zonal speed. Major currents are labeled (see text for abbreviations).

The eastern nSEC/cSEC jets are fed by recirculation from the NECC/Guinea Current in the Gulf of Guinea (Fig. 6). East of 5°W, the jets are not distinguishable—the equatorial SEC is relatively weak (~ 20 cm/s) and broad (equator to at least 7°S) east of the Greenwich Meridian. At 10°W, the nSEC is strong and significant, 37 ± 10 cm/s, on the equator (Fig. 8). At the same longitude, westward speed decreases to the south, with a plateau at 3–4°S suggesting the presence of a (not significant) cSEC. At 20°W, the two jets at 1°N (nSEC) and 5°S (cSEC) are separated by a local minimum in zonal speed which is not significantly weaker (Fig. 8). They are distinctly separated at 30°W, with the 33 ± 11 cm/s nSEC at 2°N and the 34 ± 5 cm/s cSEC at 4°S, separated by a mean eastward speed of 6 ± 12 cm/s at 1°S.

As noted above, the cSEC continues westward to join the NBC at the Brazilian coast. In contrast, most of the near-surface water in the nSEC does not reach the coast, but instead recirculates northward into the NECC. This recirculation is particularly strong in the band 30–40°W. West of this, the time-mean nSEC is weak, although there is a southward-displaced extension which reaches the Brazilian coast at 0–2°N, 43–46°W and enters the NBC east of the retroflection.

South of the cSEC jet, the sSEC is a broad, relatively weak west-southwestward flow in the total velocity field (Fig. 6). Mean westward speeds in the interior diminish approximately linearly from the 4°S cSEC core to about 8°S, where they are ~ 8 cm/s, and remain at 8–10 cm/s to the 20°S southern boundary of this study. The sSEC impinges upon South America and bifurcates, to form the northward NBC and southward Brazil Current. In the total velocity field, the latitude of this bifurcation is 12–14°S (Fig. 7, top). There is no signature of the subsurface-intensified South Equatorial Countercurrent (SECC) in the total near-surface velocity field (Molinari, 1983).

With the Ekman component removed, the interior flow is northwestward south of 12°S, consistent with schematics of the South Atlantic's subtropical gyre drawn from hydrography (e.g. Fig. 2 of Arnault, 1987 or Fig. 4 of Stramma and Schott, 1999). The Ekman-removed bifurcation latitude is at 15–17°S, consistent with the contin-

uous North Brazil Undercurrent seen in current meter moorings at 11°S and 5°S (Schott et al, 2004). East of 5°W, water entering the domain across 24°S and advected by the Ekman-removed currents (Fig. 7, bottom) turns eastward and reaches the Prime Meridian in the SECC. Averaged from 10°W–0°, the Ekman-removed zonal speed is 10 ± 5 cm/s eastward at 8°S. East of 0°, the fate of this water cannot be resolved due to low observation density. Against the Angola coast, observations are extremely scarce: only 13 drifters have sampled the region east of 10°E, 5–17°S. These drifters indicate a southward Angola Current of mean strength 6 ± 3 cm/s (2 ± 3 cm/s in total currents).

NEC: North of the NECC, total currents are nearly unidirectionally northwestward (Fig. 6), indicating little time-mean near-surface flow from the northern hemisphere's subtropical gyre into the equatorial gyre. The northward component is predominantly due to Ekman drift (Arnault, 1987)—with the Ekman component removed, interior flow in the NEC has a southward component, bifurcating against the Brazilian coast at 56°W. East of this bifurcation, the sub-Ekman NEC turns eastward along the northern edge of the NECC (Fig. 7, bottom). It is currently impossible to determine the fate of this pathway as it nears the African coast. Some fraction may join the Guinea Current as suggested in Fig. 7 (bottom), while the rest flows northward in the eastern edge of the Guinea Dome, but in this region the observations are too sparse and potential errors in the Ekman model (Fig. 4) are large.

5. Seasonal variations

Snapshots of the near-surface currents for a climatological yearday may be reconstructed from the time-mean fields and the amplitudes and phases of the seasonal components given by the least squares decomposition. Fig. 9 shows total currents for 1 April and 1 November, extrema in the seasonal cycle of the western NECC. Only a subset of the domain is shown in order to focus upon the western tropical Atlantic. For this figure,
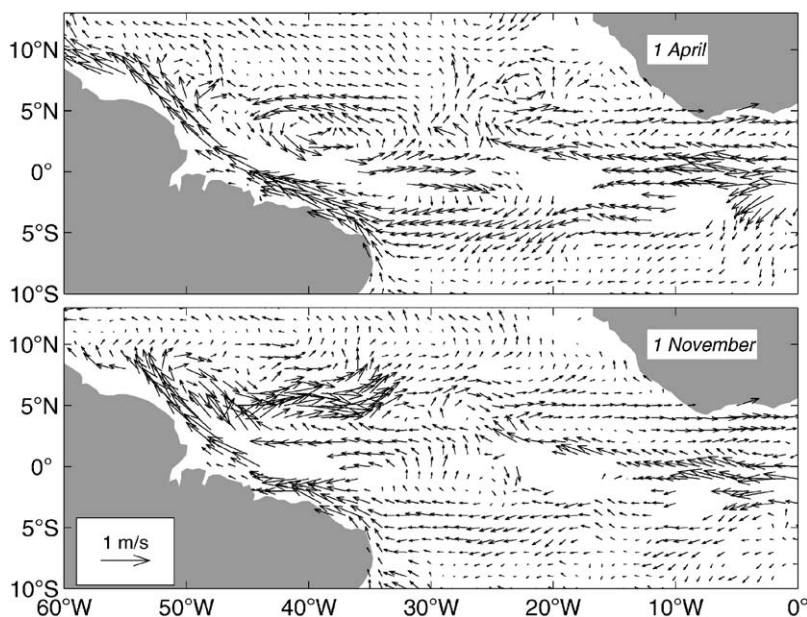
Fig. 9. Climatological near-surface currents (quivers) for 1 April (top) and 1 November (bottom), smoothed by optimal interpolation (see text).

the fields have been smoothed via Optimum Interpolation (OI), assuming a Gaussian autocorrelation function of length scale 150 km (Gandin, 1963; Cuny et al., 2002). In early November, most of the near-surface water in the NBC retroflects and flows eastward to the western NECC (Richardson and Reverdin, 1987; Carton and Katz, 1990), which concurrently reaches its maximum seasonal strength (Fig. 10). Northwest of the retroflection, the Guyana Current drops to its minimum strength in mid-August (21 ± 30 cm/s westward), and does not strengthen significantly until late February. From January to April, the NBC retroflection and western NECC weaken. By early April, the retroflection has almost disappeared in total near-surface currents (Fig. 9), although it is present throughout the year in Ekman-removed currents (Fig. 10). There is no evidence of seasonal migration of the retroflection latitude, consistent with observations from an array of inverted echo sounders (Garzoli et al., 2004). During boreal winter the western nSEC and NECC also weaken, the latter disappearing in February–March and reversing to a peak westward speed of 49 ± 20 cm/s in early April. This

reversal is also present in the Ekman-removed currents, which reach a peak westward speed of 25 ± 20 cm/s in mid-late April (Fig. 10, bottom). The seasonal cycle of western NECC Ekman-removed currents can be compared to geostrophic currents from altimetry, inverted echo sounders, and climatological dynamic height during November 1987–October 1989 (Carton and Katz, 1990); discrepancies would indicate significant ageostrophic motion, errors in the Ekman model, or discrepancies due to interannual variability. Zonal geostrophic currents at 5–6°N, 38°W (Fig.7a, middle panel of Carton and Katz, 1990) reached minima of 20–25 cm/s westward in March 1988 and 0–10 cm/s westward in May–June 1989, somewhat weaker than the Ekman-removed currents derived here (25 ± 20 cm/s westward, Fig. 10, bottom) during mid-April; they peaked at 50–70 cm/s eastward in December 1987 and 70–100 cm/s in November–December 1988, close to the drifter-derived Ekman-removed time series. The two currents' time series are consistent in phase and not significantly different in amplitude, suggesting that Ekman-removed currents are close to the geostrophic currents here.
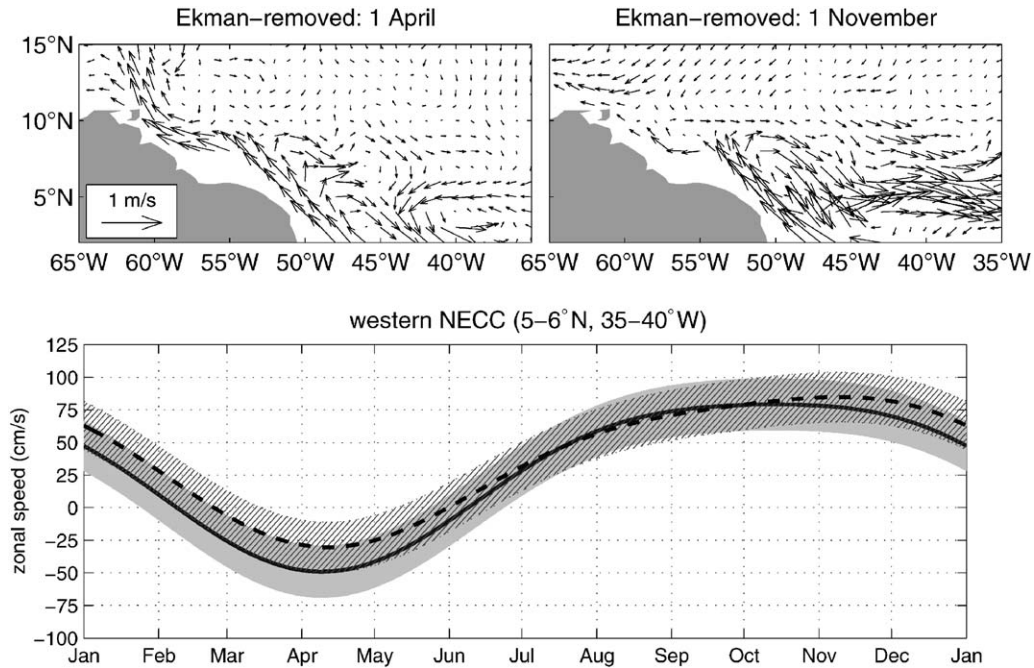
Fig. 10. *Top*: snapshots of the Ekman-removed currents during extrema of the western NECC. The currents have been smoothed as in Fig. 9. *Bottom*: seasonal variations of the western NECC (solid line: total current. dashed line: Ekman-removed current).

Concurrent with the reversals of the western nSEC and NECC, the Guyana Current strengthens, reaching its maximum westward speed of $90 \pm 30\,\text{cm/s}$ in late April. In the central Atlantic, westward Ekman drift overwhelms the eastward geostrophic signature of the NECC during boreal spring (Richardson et al., 1992): averaged in the region 5–6°N, 23–33°W, total drifter zonal speed is $15 \pm 12\,\text{cm/s}$ westward in mid-March, while the concurrent Ekman-removed speed is $3 \pm 11\,\text{cm/s}$ eastward. High salinity and relatively low oxygen in this sub-Ekman eastward flow indicates that, during the spring reversal of the western NECC, it is fed by water recirculating from the NEC (Bourlès et al., 1999).

5.1. Distribution of amplitudes

The amplitude A of a seasonal harmonic can be expressed as $A = 1/2(A_x^2 + A_y^2)^{1/2}$, where x and y denote the zonal and meridional components (Richardson and Walsh, 1986). The distributions of the annual and semiannual amplitudes of near-surface currents derived from the drifter observations are shown in Figs. 11 and 12. At basin scale the amplitudes are distributed qualitatively similar to those derived from ship drifts (Fig. 6 of Richardson and Walsh, 1986) and altimetry (Fig. 5 of Stramma et al., 2003): annual amplitudes are largest in the western tropics north of the equator, and semiannual amplitudes are largest in the central and eastern basin at 0–2°N. The phase distribution of these components (not shown) is also qualitatively consistent with earlier studies. However, many details of Figs. 11 and 12 are novel for in situ current measurements, primarily due to the five-fold increase in spatial resolution offered by the drifter observations compared to the ship drifts.

Annual amplitude (Fig. 11) is high in an elongated C-shaped feature which encompasses the nSEC, NBC retroflection, NECC and Guinea Current. Amplitudes are relatively small ($<10\,\text{cm/s}$) in the central Atlantic along
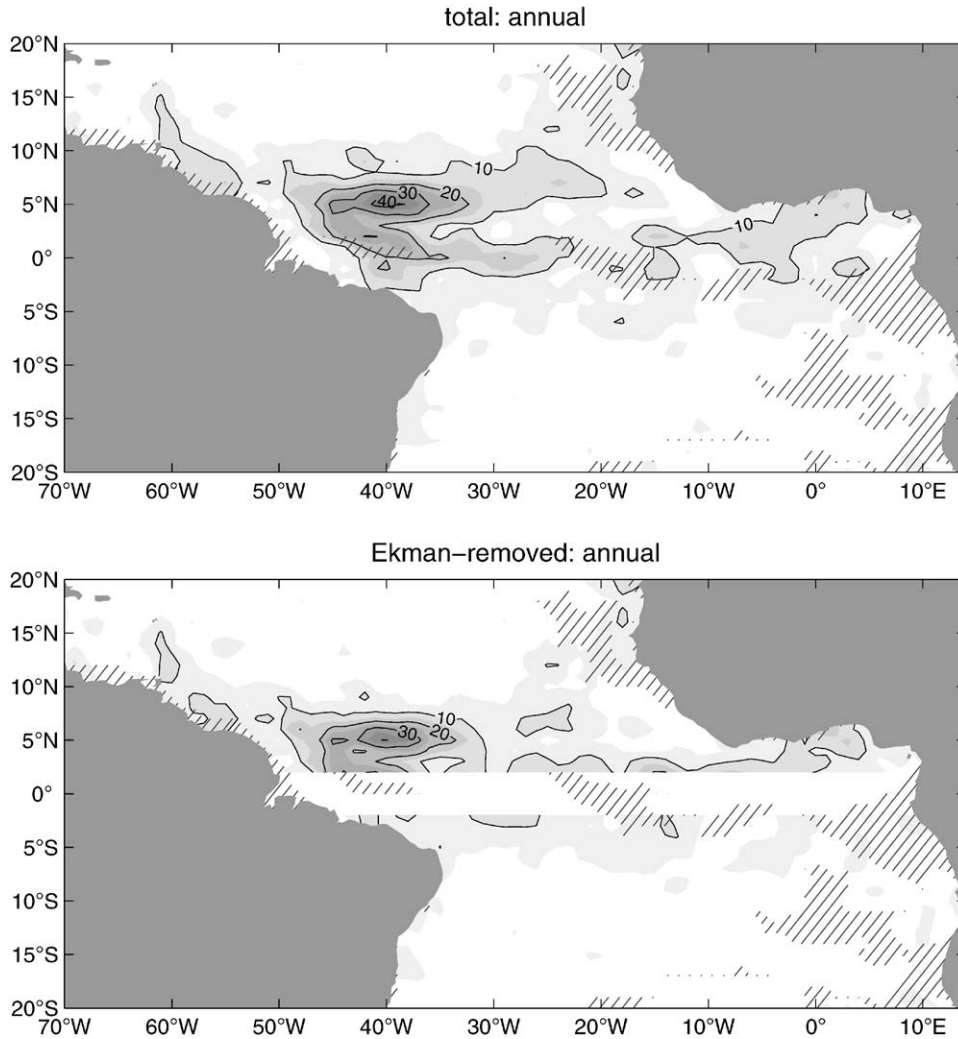
Fig. 11. Amplitude of the annual component of total (top) and Ekman-removed (bottom) velocity. Hatched areas indicate where observation density is lower than 20 drifter-days per bin. Line contours are shown for ever 10 cm/s (every 5 cm/s shaded).

4°N (between the nSEC and NECC), within most of the coastal bins of the NBC, and in the majority of bins north of 10°N or south of 3°S. This C-shaped structure was not resolved by ship drifts (Fig. 6 of Richardson and Walsh, 1986) which instead showed annual amplitudes with a broad maximum against the north Brazilian coast and extending westward along the path of the NECC, but with much smaller values (5–10 cm/s) along the nSEC. The larger drifter-derived amplitude in the western nSEC is consistent with its boreal spring

reversal inferred from SEQUAL/FOCAL drifter trajectories (Richardson and Reverdin, 1987) and confirmed by the drifters analyzed here (Fig. 9, bottom).

The largest annual amplitudes are observed in the western NECC (Fig. 11, top): five of the overlapping $2° \times 1°$ bins (at 5°N, 39–44°W) contain values > 40 cm/s, far larger than the 23 cm/s co-located maximum determined from ship drifts (Richardson and Walsh, 1986). This difference is partially due to resolution. Smoothed at
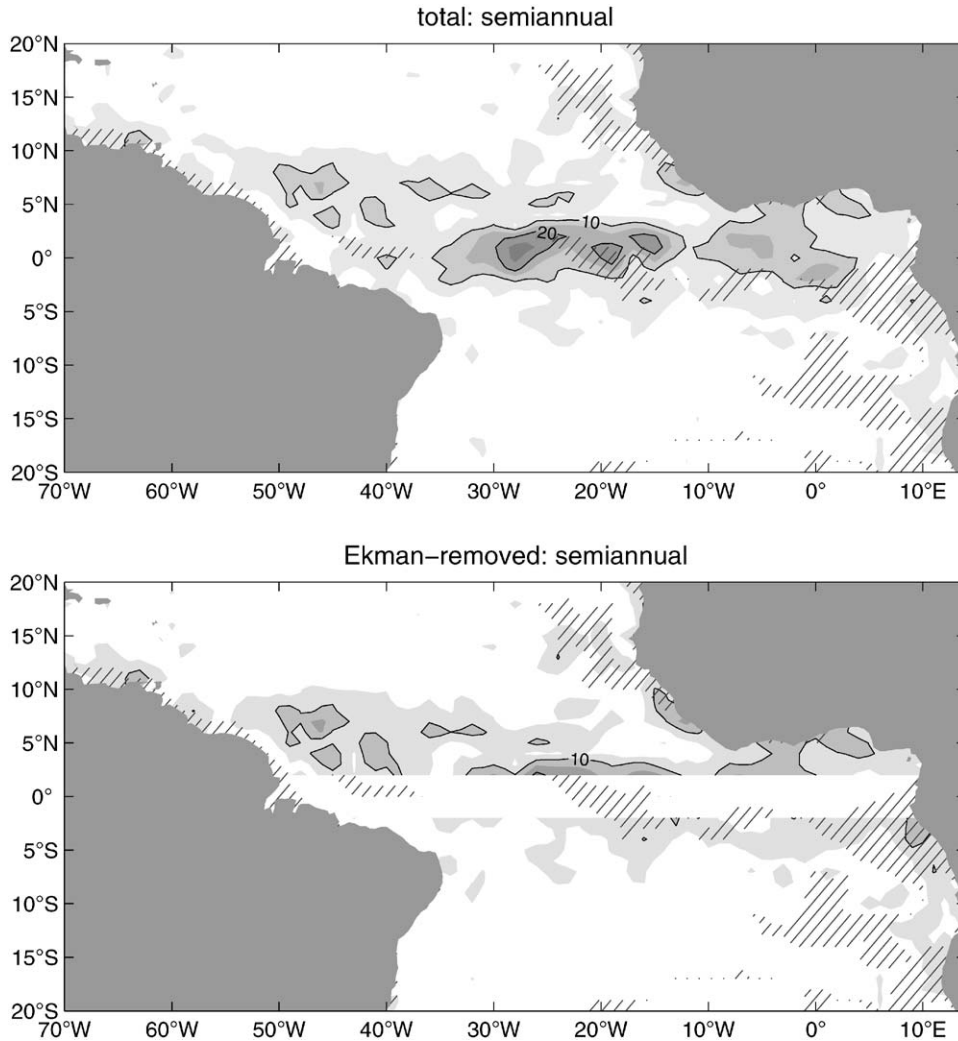
Fig. 12. Amplitude of the semiannual component of total (top) and Ekman-removed (bottom) velocity. Hatched areas indicate where observation density is lower than 20 drifter-days per bin. Line contours are shown for ever 10 cm/s (every 5 cm/s shaded).

2° meridional resolution, drifter-derived amplitudes in these bins drop to 30–35 cm/s. In addition, direct wind forcing may reduce the amplitudes in the ship drift results. In the latitude band 4–12°N, trade winds over the western Atlantic are strongest in boreal fall and weakest in spring, suggesting an annual variation of direct wind forcing which opposes that of the western NECC.

Annual amplitudes of the Ekman-removed velocities (Fig. 11, bottom) indicate that most of this variability extends below the Ekman layer.

Ekman-removed annual amplitudes are >70% of those derived from total velocity in all regions except the eastern NECC (15–34°W) and the eastern Guyana Current (54–58°W, 6–7°N). The C-shaped distribution seen in total currents is present in the Ekman-removed currents, and is consistent with the primary EOF of seasonal sea level anomaly (SLA) variations (Arnault et al., 1999) which has maximum amplitudes along 3–4°N, 30–40°W. The primarily annual SLA extreme of this mode correspond to maximum

gradients (zonal geostrophic currents) north (NECC) and south (nSEC) of this band. The distribution of annual amplitudes from altimetry-derived geostrophic currents (Stramma et al., 2003; their Fig. 5) in the zonal band 20–35°W is consistent with our Ekman-removed annual amplitudes in distribution (including the C-shaped maximum) and magnitude.

Semiannual amplitudes are high along the nSEC and against the Guinea coast (Fig. 12), on and north of the equator. These strong semiannual fluctuations are a resonant response to the semiannual component of equatorial wind forcing in the eastern Atlantic (Philander and Pacanowski, 1986). The largest semiannual amplitudes are found at 1°S–2°N, 15–30°W, where they are 20–30 cm/s. Co-located semiannual amplitudes derived from ship drifts (Richardson and Walsh, 1986) were < 12 cm/s. This discrepancy is dramatic, and is not due solely to increased resolution—even when smoothed in the bins of the ship drift study, drifter-derived semiannual amplitudes are 16–21 cm/s in the six bins spanning this region.[1]

One might hypothesize that the discrepancy between ship drift and drifter-derived semiannual amplitudes in the central equatorial band is due to direct wind forcing biasing the ship drifts, as proposed earlier for annual amplitudes in the western NECC. However, although wind variability includes a semiannual component east of 30°W, any directly wind-forced bias in ship drifts should be in phase with the oceanic response (Philander and Pacanowski, 1986); i.e. this effect, if significant, should produce *larger* semiannual amplitudes from ship observations than from drifters.

An alternative hypothesis is that the drifter-derived semiannual amplitude in this region has been aliased by higher-frequency variability. This could be caused by non-random drifter deployments, e.g. preferential seeding of a mesoscale feature, or nonrandom sampling due to horizontal convergence associated with such a feature. An

obvious candidate for this is tropical instability wave (TIW) variability. Drifters orbiting a TIW would exhibit anomalous westward currents near the equator (e.g., Menkes et al., 2001). However, the primary difference between drifter-derived and ship drift-derived seasonal currents here is that the drifters indicate strong *eastward* currents near the equator during boreal spring, not present in ship drift results. These eastward currents can be seen in a time-latitude plot of zonal speed averaged in the band 23–33°W (Fig. 13; contrast to Fig. 8 of Richardson and Philander, 1987). Nearly 90% of the March–May drifter observations in the region 23–33°W, 2°S–2°N were collected in the years 1999 (eight drifters) and 2002 (six drifters). Their trajectories (cf. Fig. 13, bottom) suggest an eastward, zonally extended jet, rather than the southern edge of orbits around a TIW.
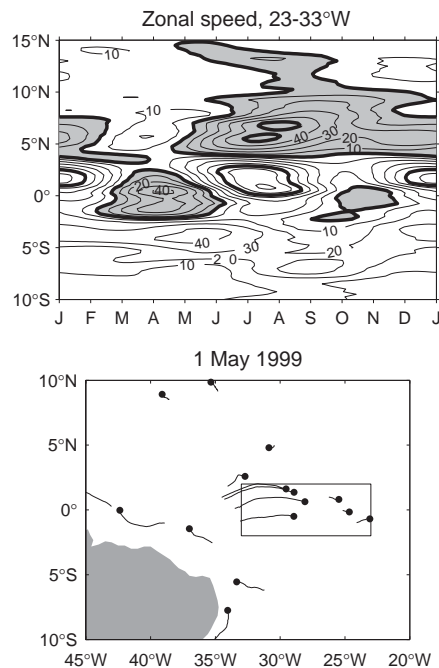

Fig. 13. *Top*: total near-surface drifter speeds (cm/s) between 23 and 33°W, plotted vs. month. Shading indicates positive (eastward) speeds. Every 10 cm/s contoured. *Bottom*: location of drifters on 1 May 1999 (bullets) and the trajectory over the previous 10 days. Drifters east of 26°W were deployed less than 10 days earlier. The area 2°S−2°N, 23−33°W is indicated by a rectangle.

---

[1]In contrast, smoothed semiannual amplitudes off the Guinea coast are consistent with ship drift results, which were largest there.

A third hypothesis for this discrepancy is interannual variability, which is much larger in the nSEC than in the NECC (Richardson and Reverdin, 1987). The ship drifts span many years, and are particularly dense during 1920–1940, but are extremely spatially inhomogeneous near the equator: east of 30°W they are effectively confined to the major shipping routes at 20°W and 8°W. In contrast, most (83%) of the more spatially homogeneous drifter observations in this region (2.0 drifter years in 1°S–2°N, 15–30°W) are in the years 1998–2000, 2002–2003.

Finally, we note that mean ship drifts fail to resolve the nSEC and enhanced annual amplitudes in the equatorial band, both of which are robust features in the drifter data and in the other observations-cited earlier. Conceivably, related sampling-related problems in the ship drift dataset may have failed to resolve the near-surface manifestation of the shoaling Equatorial Undercurrent (EUC), which is shallowest in boreal spring (Weisberg et al., 1987; Bourlès et al., 1999), consistent with the eastward jet seen in Fig. 13. Similar semiannual amplitudes (exceeding 20 cm/s in geostrophic zonal velocity anomalies) have been derived from TOPEX/POSEIDON observations (Stramma et al., 2003), although peak amplitudes were at 20–22°W, east of our 26–29°W peak. Equatorial current meter observations at 28°W during SEQUAL/FOCAL (Weisberg et al., 1987) are qualitatively consistent with the drifter observations: above the 50–100 m core of the EUC, lowpassed zonal speeds are generally eastward during March–April and westward during June–July and December–January. Those authors do not report the semiannual amplitude from their 2.7 year time series of 10 m currents, precluding quantitative comparison with the drifter results, although the time series (Fig. 1 of Weisberg et al., 1987) suggests an amplitude smaller than the 15.7 ± 5.4 cm/s drifter-derived value in the region 1°S–2°N, 15–30°W. Of course, interannual variability could be invoked to account for discrepancies, and current meter results describe a much smaller region, sampled far more homogeneously, than the area integrated by the drifters. Longer in situ time series are needed in order to resolve variability at these time scales.

5.2. EOF analysis

To quantify the dominant patterns of seasonal variability, the annual-plus-semiannual currents $\boldsymbol{u}_s(t)$ were expanded in terms of empirical orthogonal functions (EOFs; Wallace and Dickinson, 1972). Within each bin, the principal component axis (PCA) of $\boldsymbol{u}_s = (u_s, v_s)$ was determined. In most bins this axis was aligned with the time-mean velocity. The component of $\boldsymbol{u}_s$ along this axis was expanded into EOFs. The first three EOFs
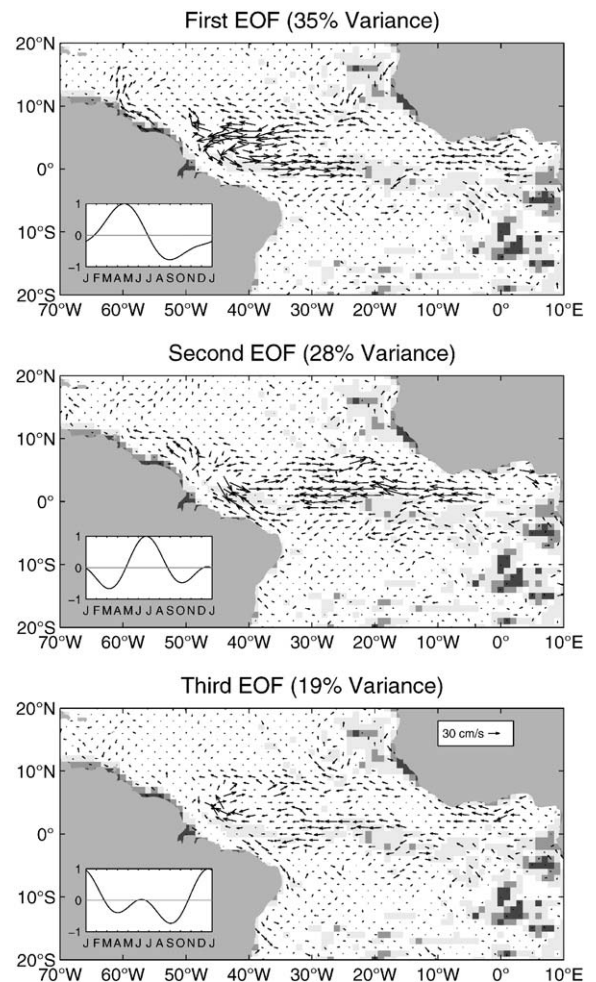

Fig. 14. First three EOFs of the seasonal variations of total near-surface currents. Arrows indicate the magnitude and phase; insets show the time series corresponding to the spatial patterns. Quivers are shown for every other bin; EOFs calculated for all bins.

(Fig. 14) account for 82% of the overall annual-plus-semiannual variability along the PCA (hereafter called the "seasonal variability"). The first two EOFs qualitatively resemble those derived from monthly mean ship drifts (Fig. 9 of Richardson and Walsh, 1986) in the fraction of variance explained, the distribution of amplitude, and the time series of the modes.

The first drifter EOF (35% of the seasonal variance) is primarily annual, associated with the boreal fall strengthening of the western NECC/nSEC and NBC retroflection, and the spring reversal of the western NECC/nSEC and weakening of the retroflection. Extrema of this mode were shown in Fig. 9. This mode corresponds to the equilibrium oceanic response to the annual variation of the winds (Philander and Pacanowski, 1986). In the western tropics, where the EOF's amplitudes are largest, the wind stress curl reverses during boreal spring. This reversal forces thermocline depth changes consistent with the reversing NECC (Garzoli and Katz, 1983) and nSEC (Katz et al., 1981). Significant amplitudes extend eastward along the NECC to the Guinea Coast, consistent in phase with the acceleration/deceleration of the western NECC. The mode's amplitude distribution along the NECC, along with its phase, is consistent with the primary EOF of sea height anomaly across 2–10°N (Katz et al., 1995). The drifter-derived EOF's phase reverses along the path of the equatorial nSEC, somewhere within the poorly sampled band 13–23°W, consistent with the first EOF from ship drifts (Richardson and Walsh, 1986).

South of the equator, the first drifter EOF is not a strong signal along the NBC. This result is inconsistent with the ship drift-derived first EOF. However, the mode dominates seasonal variations of the NBC north of the equator. We interpret this as follows: in the time-mean field (Fig. 6), the westernmost nSEC feeds into the NBC at 0–2°N. The spring reversal of this current deprives the NBC of this input. Downstream, at 4°N, current meter (Johns et al., 1998) and inverted echo sounder (Garzoli et al., 2004) observations show that the NBC's transport drops to its minimum in April–May. Further downstream along the Guyana coast, the first drifter EOF has large amplitudes

from the retroflection to ∼ 60°W. Here this signal leaves the coast and turns northward east of the Lesser Antilles, and thus does not penetrate into the Caribbean Sea. Phase along this pathway indicates that its transport is *largest* during spring months—less water may be arriving at the mean location of the retroflection, but the seasonally weakened retroflection siphons off less water than during fall months. This seasonal "switch" between the retroflection and Guyana Current was suggested by several SEQUAL/FOCAL drifter trajectories (Richardson and Reverdin, 1987), but was not clearly resolved by ship drifts. Its existence is verified by these much denser observations.

The distribution of the second EOF's amplitude and phase indicates a central-to-eastern intensified spin up/slow down of the equatorial gyre system (Richardson and Walsh, 1986). However, it is difficult to physically interpret this mode in isolation, except where it dominates the seasonal signal. Amplitudes of the second EOF are more than twice those of the first or third EOF in two regions: the nSEC and cSEC at 0–30°W, 5°S–3°N, and the westward-flowing portion of the NBC from 4°S, 37°W (north of the easternmost point of Brazil) to the equator. The second and third EOFs have large amplitudes in the western nSEC, where they are in phase. The superposition of these modes is consistent with the strong semiannual variations of the western nSEC noted earlier. The amplitudes of these modes are also large (combined 20–30 cm/s) in the region where the sSEC impinges upon the Brazilian coast and bifurcates. The phase of these two modes is in opposition here, and along the paths of the NBC (to 4°S) and Brazil Current, indicating primarily annual variations with maximum speeds in July. This variability is presumably driven by variations in the strength of the wind-driven South Atlantic subtropical gyre, which is magnified in its western boundary currents. This annual cycle, with extrema in winter/summer, is out of phase with the spring/fall equilibrium response of the near-equatorial Atlantic to local wind forcing. Thus, it does not project onto the first EOF, unlike in the ship drift analysis of Richardson and Walsh (1986).

The third EOF accounts for twice as much variance as in the ship drift analysis (Richardson

and Walsh, 1986). Richardson and Walsh did not present their third EOF, which they describe as noisy and lacking obvious large-scale patterns. Perhaps due to the more homogeneous distribution of drifter observations, the third EOF derived here appears to be much less noisy, although it does not dominate seasonality anywhere within the domain.

6. Summary

Observations collected by drifters in the tropical Atlantic Ocean as part of the Global Ocean Observing System, analyzed by a methodology designed for inhomogeneous, seasonally varying data, have shed new light upon our knowledge of the near-surface mean currents and their seasonal variability. Previous climatologies of in situ-observed currents were derived from ship drifts, which are prone to systematic bias from direct wind forcing and are distributed much more inhomogeneously throughout the tropics (i.e., most are along major shipping routes). Decomposition of the drifter observations into time-mean and seasonal components allows the derivation of a new climatology of monthly tropical Atlantic currents and sea-surface temperature at unprecedented resolution (available for download at http://www.aoml.noaa.gov/phod/dac/drifter_climatology.html). These monthly mean fields are a climatology for the time period 1997—present, the period during which the tropical Atlantic drifter array has been maintained.

Due to the tremendous recent increase in the density of drifter observations, time-mean and seasonal amplitudes of the near-surface circulation were resolved at much higher resolution than in previous studies. These data now reveal the bifurcation of the sSEC against the South American coast and the separation of the nSEC and cSEC branches. The westward flowing southern branch of the SEC bifurcates south of the westernmost tip of the South American continent. North of the bifurcation, a weak coastal current (the NBC) gains strength as it is fed by the SEC inflow and is joined by the central SEC branch at $\sim 4°$S. The confluence of these currents accelerates

the NBC, which is further enhanced when it is joined by the westernmost extension of the SEC's northern branch at 2–3°N. Further northwest, the NBC retroflects while a narrow Guyana Current, which extends below the Ekman layer, continues along the coast. The westward speed of the Guyana Current strengthens in concert with the seasonal weakening of the NBC retroflection and reversal of the western NECC.

The drifter observations clearly resolve the NBC retroflection between 50 and 54°W, continuity between the retroflection and the western NECC, and the covarying seasonality of these currents' strength. The mean NECC is not a continuous advective pathway at the ocean surface, as a strong northward Ekman drift carries parcels out of the western NECC and into the southern edge of the NEC. When the Ekman component is removed, the NECC becomes a continuous eastward advective pathway, and velocities within the NEC suggest a recirculation from the northern hemisphere subtropical gyre into the NECC below the Ekman layer.

Basin-scale features of the currents' seasonal variability are qualitatively similar to results from an analysis of ship drifts (Richardson and Walsh, 1986). For example, annual amplitudes are largest in the western tropics north of the equator, and semiannual amplitudes are largest in the central and eastern basin at 0–2°N. This qualitative similarity is a remarkable result given the differences in the platforms and in the time periods (ship drifts biased towards 1920–1940, drifters for 1997—present). However, significant differences are observed both in the magnitudes and the distributions of these amplitudes. The drifters reveal considerably more structure to the distribution of annual amplitudes, which are elevated in an elongated C-shaped feature encompassing the NECC, Guinea Current, NBC retroflection and the nSEC. Semiannual amplitudes are elevated along the nSEC, reaching maxima in the central basin which are twice as large as those derived from ship drifts. The increase in resolution offered by the drifters is due to the greater spatial homogeneity of their observations, as they are not confined to the major shipping routes.

The first orthogonal mode describing the currents' seasonal variability is associated with the direct oceanic response to the primarily annual variation of wind stress curl in the tropics. This mode describes seasonal variations in the strength of the NBC retroflection, Guyana Current, and western NECC/nSEC. The inverse variations in the strengths of the retroflection and Guyana Current suggest a connection between the equatorial gyre and the northern hemisphere subtropical gyre via the Guyana Current conduit. The second orthogonal mode dominates seasonal variations in the cSEC, a region where Reverdin and McPhaden (1986) highlighted discrepancies between ship drift climatology and FOCAL drifter observations. FOCAL drifters indicated that zonal speed dropped to zero in February–April, while the climatology indicated mean westward speeds of 20 cm/s. Westward drifter speed in the cSEC (3–7°S, 10–30°W) weaken to minima of 18 ± 5 cm/s in early April and November and peak at 8 ± 5 cm/s in mid-July. This result is consistent with the climatology, and with Reverdin and McPhaden's hypothesis that the 1984 FOCAL observations were anomalous due to the El Niño conditions of that year. The second and third orthogonal modes are associated with a resonant response to semiannual variations in equatorial wind forcing (Philander and Pacanowski, 1986), and with the response to annual variations in South Atlantic wind stress which connects the southern hemisphere subtropical gyre to the equatorial gyre via the NBC conduit. Both processes modulate the strength of the various SEC branches, and the resulting variability is transmitted to the NBC as these branches form or join with it.

7. Conclusions

One of the major findings of this study is the significant, inverse fluctions in the strenghts of the Guyana Current and NBC retroflection. This result has been implied in many earlier studies (Richardson and Walsh, 1986; Richardson and Reverdin, 1987; Bourlès et al., 1999), but limited observations or spatial resolution have tended to

obscure it or render its downstream fate uncertain. The gridded currents presented in the previous sections do not address whether the Guyana Current is a "true" current, i.e. a coastal current extending from the NBC retroflection to the Caribbean, or is instead the time-mean pathway of NBC retroflection rings carrying the drifters westward. To address this issue, the drifters which passed near the Guyana coast (shaded region in Fig. 15, top), and continued north or west rather than retroflecting, were sorted into two categories: loopers (drifters making two or more consecutive loops and/or cusps, associated with rotation within a ring; Richardson, 2004) and non-loopers. Thirty-two of the drifters were loopers. Most of these continued orbiting rings after they left the South American coast and propagated northward, east of the Lesser Antilles, while six loopers left the rings (ceased looping) and entered the Caribbean Sea south of Puerto Rico. In contrast, 14 of the 16 non-loopers entered the Caribbean Sea south of Puerto Rico (for a recent examination of drifters in the Caribbean Sea, see Richardson, 2004). These results indicate that NBC ring propagation is a major contributor to the "Guyana Current", but the relative numbers of loopers and non-loopers must be interpreted cautiously. The 1998–2000 NBC Rings Experiment (NBCRE; see Section 2) seeded rings with drifters, introducing a bias to the number of loopers vs. non-loopers here. Excluding drifters deployed during the NBCRE, 15 of the Guyana coast drifters were loopers and 12 were non-loopers. Seasonal-mean currents calculated from all non-NBCRE drifters (Fig. 15, bottom) are qualitatively similar to the currents calculated from all drifters, indicating that the Guyana Current bifurcates at $\sim 60°$W, with a northward branch associated with NBC ring propagation and a southward branch which enters the Caribbean between the South American coast and $\sim 15°$N, associated with non-looping drifter trajectories.

This study has focused upon the time-mean circulation and its seasonal variability. A future paper will examine the residual fluctuations determined by the least-squares decomposition, which are predominantly due to mesoscale eddies and rings, equatorial waves, and interannual variability. These fluctuations set the time scales
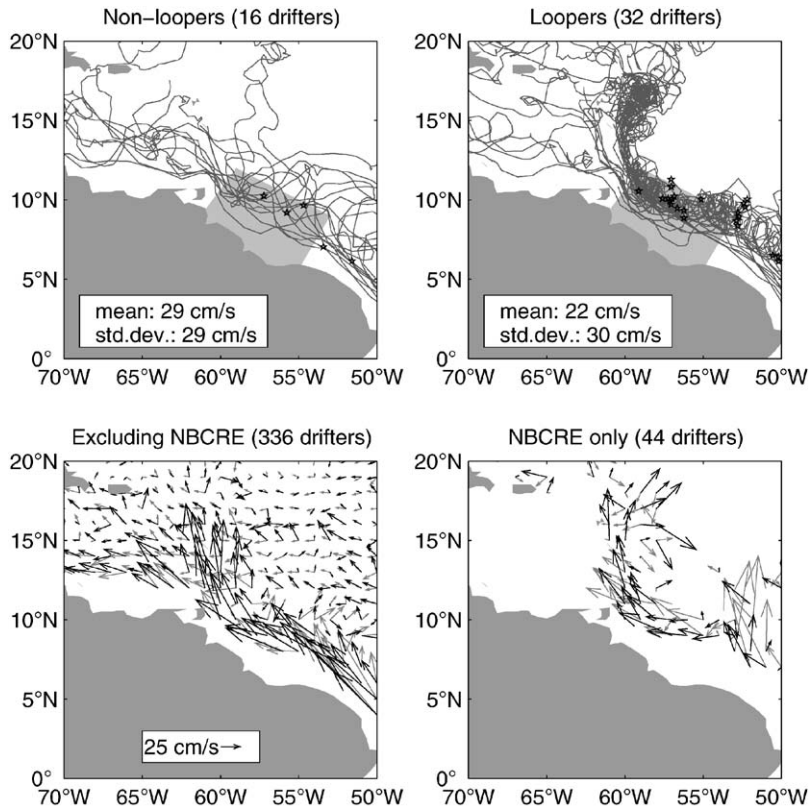
Fig. 15. *Top*: trajectories of non-loopers (left) and loopers (right) which passed through the Guyana coast region (shaded) and continued west or north. Drifter trajectories which retroflected are not shown. Stars indicate deployment locations. Inset gives the mean alongshore current (the component 30° north of due west) in the Guyana coast region, and its standard deviation. *Bottom*: climatological currents for 1 November (gray) and 1 April (black) calculated for drifters launched as part of the NBC Rings Experiment (right) and all non-NBCRE drifters (left). Currents are not shown where there are <20 drifter days.

of dispersion and may generate momentum fluxes which transfer energy between the eddy-scale features and the larger scale circulation features examined here. Additional future efforts will combine the currents and temperatures given by the decomposition with various subsurface data, in order to compute the role of advection in the heat budget of the tropical Atlantic Ocean.

References

Arnault, S., 1987. Tropical Atlantic geostrophic currents and ship drifts. Journal of Physical Oceanography 18, 1050–1060.

Arnault, S., Bourlès, B., Gouriou, Y., Chuchla, R., 1999. Intercomparison of the upper layer circulation of the western equatorial Atlantic Ocean: In situ and satellite data. Journal of Geophysical Research 104 (C9), 21171–21194.

Bourlès, B., Gouriou, Y., Chuchla, R., 1999. On the circulation in the upper layer of the western equatorial Atlantic. Journal of Geophysical Research 104 (C9), 21151–21170.

Carton, J.A., Katz, E.J., 1990. Estimates of the zonal slope and seasonal transport of the Atlantic North Equatorial Countercurrent. Journal of Geophysical Research 95 (C3), 3091–3100.

Cuny, J., Rhines, P.B., Niiler, P.P., Bacon, S., 2002. Labrador Sea boundary currents and the fate of the Irminger Sea Water. Journal of Physical Oceanography 32 (2), 627–647.

Didden, N., Schott, F., 1993. Eddies in the North Brazil Current retroflection. Journal of Geophysical Research 98, 20121–20131.

Fratantoni, D.M., 2001. North Atlantic surface circulation during the 1990's observed with satellite-tracked drifters. Journal of Geophysical Research 106, 22067–22093.

Gandin, L.S., 1963. Objective Analysis of Meteorological Fields. Hydromet Press.

Garzoli, S.L., 1992. The Atlantic North Equatorial Countercurrent models and observations. Journal of Geophysical Research 97 (C11), 17931–17946.

Garzoli, S.L., Katz, E.J., 1983. The forced annual reversal of the Atlantic North Equatorial Countercurrent. Journal of Physical Oceanography 13, 2082–2090.

Garzoli, S.L., Yao, Q., Ffield, A., 2003. North Brazil Current rings and the variability in the latitude of retroflection. In: Goni, G., Malanotte-Rizzoli, P., (Eds.), Interhemispheric Water Exchange in the Atlantic Ocean. Elsevier Oceanographic Series, pp. 357–374.

Garzoli, S.L., Ffield, A., Johns, W.E., Yao, Q., 2004. North Brazil Current retroflection and transports. Journal of Geophysical Research 109, C01013 (doi:10.1029/2003JC001774).

Glickson, D.A., Fratantoni, D.M., Wooding, C.M., Richardson, P.L., 2000. North Brazil Current rings experiment: surface drifter data report, November 1998–June 2000. Technical Report WHOI-2000-10, Woods Hole Oceanographic Institution.

Hansen, D., Herman, A., 1989. Temporal sampling requirements for surface drifting buoys in the tropical Pacific. Journal of Atmospheric and Oceanic Technology 6, 599–607.

Hansen, D., Poulain, P.-M., 1996. Quality control and interpolations of WOCE-TOGA drifter data. Journal of Atmospheric and Oceanic Technology 13, 900–909.

Johns, W.E., Lee, T.N., Beardsley, R.C., Candela, J., Limeburner, R., Castro, B., 1998. Annual cycle and variability of the North Brazil Current. Journal of Physical Oceanography 28, 103–128.

Johnson, G.C., 2001. The Pacific Ocean subtropical cell surface limb. Geophysical Research Letters 28 (9), 1771–1774.

Josey, S.A., Kent, E.C., Taylor, P.K., 2002. On the wind stress forcing of the ocean in the SOC climatology: comparisons with the NCEP/NCAR, ECMWF, UWM/COADS and Hellerman and Rosenstein datasets. Journal of Physical Oceanography 32, 1993–2019.

Katz, E.J., Molinari, R.L., Cartwright, D.E., Hisard, P., Lass, H.U., deMesquita, A., 1981. The seasonal transport of the equatorial undercurrent in the western Atlantic (during the Global Weather Experiment). Oceanologica Acta 4, 445–450.

Katz, E.J., Carton, J.A., Chakraborty, A., 1995. Dynamics of the equatorial Atlantic from altimetry. Journal of Geophysical Research 100 (C12), 25061–25067.

Lagerloef, G.S.E., Mitchum, G.T., Lukas, R.B., Niiler, P.P., 1999. Tropical Pacific near-surface currents estimated from altimeter, wind and drifter data. Journal of Geophysical Research 104 (C10), 23313–23326.

Lumpkin, R., 1998. Eddies and Currents of the Hawaiian Islands. Ph.D. Thesis, University of Hawaii at Manoa, Honolulu, 281p.

Lumpkin, R., 2003. Decomposition of surface drifter observations in the Atlantic Ocean. Geophysical Research Letters 30 (14), 1753 (10.1029/2003GL017519).

Lumpkin, R., Garraffo, Z., 2005. Evaluating the decomposition of tropical Atlantic drifter observations. Journal of Atmospheric and Oceanic Technology, submitted.

Menkes, C., Kennan, S., Flament, P., Dandonneau, Y., Masson, S., Biessy, B., Marchal, E., Eldin, G., Grelet, J., Montel, Y., Morliere, A., Lebourges, A., Moulin, C., Champalbert, G., Herbland, A., 2001. A whirling ecosystem in the equatorial Atlantic. Geophysical Research Letters 29 (10.1029/2001GL014576).

Molinari, R.L., 1982. Observations of eastward currents in the tropical South Atlantic Ocean: 1978–1980. Journal of Geophysical Research 87, 9707–9714.

Molinari, R.L., 1983. Observations of near-surface currents and temperature in the central and western Tropical Atlantic Ocean. Journal of Geophysical Research 88 (C7), 4433–4438.

Nath, J.H., 1977. Wind tunnel tests on drogues. Technical Report, NOAA Data Buoy Office.

Niiler, P., 2001. The world ocean surface circulation. In: Siedler, G., Church, J., Gould, J. (Eds.), Ocean Circulation and Climate, International Geophysics Series, vol. 77. Academic Press, New York, pp. 193–204.

Niiler, P.P., Paduan, J.D., 1995. Wind-driven motions in the northeast Pacific as measured by Lagrangian drifters. Journal of Physical Oceanography 25, 2819–2830.

Pazan, S.E., Niiler, P.P., 2000. Recovery of near-surface velocity from undrogued drifters. Journal of Atmospheric and Oceanic Technology 18, 476–489.

Peterson, R.G., Stramma, L., 1991. Upper-level circulation in the South Atlantic Ocean. Progress in Oceanography 26, 1–73.

Philander, S.G.H., Pacanowski, R.C., 1986. A model of the seasonal cycle in the tropical Atlantic Ocean. Journal of Geophysical Research 91 (C12), 14192–14206.

Poulain, P.-M., Niiler, P., 1989. Statistical analysis of the surface circulation in the California Current System using satellite-tracked drifters. Journal of Physical Oceanography 19, 1588–1603.

Ralph, E.A., Niiler, P.P., 1999. Wind-driven currents in the Tropical Pacific. Journal of Physical Oceanography 29, 2121–2129.

Reverdin, G., McPhaden, M.J., 1986. Near-surface current and temperature variability observed in the equatorial Atlantic from drifting buoys. Journal of Geophysical Research 91 (C5), 6569–6581.

Richardson, P., 2004. Caribbean current and eddies as observed by surface drifters. Deep Sea Research, submitted for publication.

Richardson, P.L., McKee, T.K., 1984. Average seasonal variation of the Atlantic equatorial currents from historical ship drift. Journal of Physical Oceanography 14 (7), 1226–1238.

Richardson, P., Philander, S.G.H., 1987. The seasonal variations of surface currents in the tropical Atlantic Ocean: a comparison of ship drift data with results from a general circulation model. Journal of Geophysical Research 92 (C1), 715–724.

Richardson, P., Reverdin, G., 1987. Seasonal cycle of velocity in the Atlantic North Equatorial Countercurrent as measured by surface drifters current meters and ship drifts. Journal of Geophysical Research 92 (C4), 3691–3708.

Richardson, P., Walsh, D., 1986. Mapping climatological seasonal variations of surface currents in the Tropical Atlantic using ship drifts. Journal of Geophysical Research 91 (C9), 10537–10550.

Richardson, P.L., Arnault, S., Garzoli, S., Bruce, J.G., 1992. Annual cycle of the Atlantic North Equatorial Countercurrent. Deep Sea Research 39 (6), 997–1014.

Richardson, P.L., Hufford, G.E., Limeburner, R., 1994. North Brazil Current retroflection eddies. Journal of Geophysical Research 99 (C3), 5081–5093.

Schott, F.A., Zantopp, R., Stramma, L., Dengler, M., Fischer, J., Wibaux, M., 2004. Circulation and deep-water export at the western exit of the subpolar North Atlantic. Journal of Physical Oceanography 817–843.

Stramma, L., Schott, F., 1999. The mean flow field of the tropical Atlantic Ocean. Deep Sea Research 46, 279–303.

Stramma, L., Fischer, J., Brandt, P., Schott, F., 2003. Circulation, variability and near-equatorial meridional flow in the central tropical Atlantic. In: Goni, G.J., Malanotte-Rizzoli, P. (Eds.), Interhemispheric Water Exchange in the Atlantic Ocean. Elsevier, Amsterdam, pp. 1–22.

Sybrandy, A.L., Niiler, P.P., 1992. WOCE/TOGA Lagrangian drifter construction manual. WOCE Report 63, SIO Ref. 91/6, Scripps Institute of Oceanography, La Jolla, CA, 58pp.

Wallace, J.M., Dickinson, R.E., 1972. Empirical orthogonal representation of time series in the frequency domain. part i: theoretical considerations. Journal of Applied Meteorology 11, 887–892.

Weisberg, R.H., Hickman, J.H., Tang, T.Y., Weingartner, T.J., 1987. Velocity and temperature observations during the Seasonal Response of the Equatorial Atlantic experiment at $0°$, $28°W$. Journal of Geophysical Research 92 (C5), 5061–5075.

Wilson, W.D., Johns, W.E., Garzoli, S.L., 2002. Velocity structure of North Brazil Current rings. Geophyscial Research Letters 29 (8) 1029/2001GL013869.

World Climate Research Program, 1988. WOCE surface velocity program planning committee report of first meeting: SVP-1 and TOGA pan-Pacific surface current study. WMO/TD-No.323, WCRP-26, World Meteorological Organization, 33pp.

Zhang, D., McPhaden, M.J., Johns, W.E., 2003. Observational evidence for flow between the Subtropical and Tropical Atlantic: the Atlantic Subtropical Cells. Journal of Physical Oceanography 33, 1783–1797.